Structure of the Topa-semiquinone Catalytic Intermediate of Amine Oxidase as Revealed by Magnetic Interactions with Exchangeable ^2H and ^1H Nuclei

Kurt Warncke, Gerald T. Babcock, David M. Dooley, Michele A. McGuirl, and John McCracken*

Contribution from the Department of Chemistry, Michigan State University, East Lansing, Michigan 48824, and Department of Chemistry and Biochemistry, Montana State University, Bozeman, Montana 59717

Received October 4, 1993®

Abstract: Electron spin echo envelope modulation (ESEEM) and continuous wave–electron nuclear double resonance (CW-ENDOR) spectroscopies have been used selectively to characterize hyperfine interactions of aqueous solvent-exchangeable ^1H and ^2H nuclei with unpaired electron spin density in the topa-semiquinone catalytic intermediate of bovine amine oxidase. The radical was generated by anaerobic reduction of enzyme in ^2H_2O or ^1H_2O buffer with substrate benzylamine in the presence of cyanide ion. ^2H ESEEM spectra display a strong anisotropic hyperfine coupling of rhombic symmetry that is assigned to a single, exchangeable ^2H nucleus bonded α to the substrate-derived nitrogen atom that is incorporated into the cofactor during catalysis. Solvent exchange of this hydrogen dramatically influences the CW–electron paramagnetic resonance spectrum. ESEEM spectra show no evidence for deuteroxyl deuteron hyperfine coupling, suggesting that the two semiquinone oxygen atoms are deprotonated. Seven pairs of ^2H_2O exchange-sensitive hyperfine couplings are observed in the ^1H CW-ENDOR spectrum. These couplings are assigned to protons involved in hydrogen bonds to the nitrogen and the two oxygen atoms of the radical. The exchange insensitivity of the ^1H CW-ENDOR matrix line and relatively weak ^2H matrix ESEEM demonstrate that the radical is well-sequestered from solvent water. The presence of a single proton covalently bonded to a trigonal nitrogen atom, and the p_π-orbital overlap in the C–N bond, shows that the nuclear and electronic structure of the active carbon center in the topa-semiquinone resembles that of the subsequent iminoquinone intermediate.

Introduction

Bovine serum amine oxidase catalyzes the oxidative deamination of primary amines to the corresponding aldehydes, ammonia, and hydrogen peroxide.[1] This enzyme is a member of the family of copper-containing amine oxidases, which includes the plasma amine oxidase, kidney and placental diamine oxidase, and lysyl oxidase, which play key roles in amine metabolism or connective tissue maturation.[1] The enzyme is also found in the bacterium *Arthrobacter* P1.[2,3] With the exception of lysyl oxidase, the amine oxidases share a common dimeric polypeptide structure of molecular mass approximately 150 000 and incorporate two type II copper centers and two organic cofactors per enzyme.[4,5] The organic cofactor in the enzyme from bovine serum has been identified as a covalently bound hydroxyquinone, termed "topa-quinone" (**1**).[6] On the basis of sequence homologies and similar continuous wave electron paramagnetic resonance (CW-EPR), UV/visible, and resonance Raman spectroscopic properties, it is accepted that topa-quinone is the cofactor that is present in all copper-containing amine oxidases.[7,8] The topa-quinone is derived from the phenol side chain of a tyrosine residue,[9] which places the amine oxidases among an emerging class of enzymes that utilize post-translationally modified amino acid side chains as catalytic centers.[10] Unmodified tyrosine side chains have been shown to function as electron-transfer cofactors in several other enzyme systems.[11,12]

Topa-quinone in amine oxidase plays a dual role as both a center for bond-making and bond-breaking chemistry involving the amine substrate and as an electron-transfer cofactor. Events at the topa-quinone active site that accompany the reductive phase of the reaction sequence, as well as one step of the oxidative phase, are depicted in Figure 1. Extensive study of the reductive phase, which can proceed in the absence of dioxygen, has led to proposals that the topa-quinone mediates a sequence of addition/elimination reactions[5,13,14] that proceed through Schiff-base intermediates,[15,16] in common with mechanisms of enzyme-catalyzed and solution transamination reactions.[17] During the reductive phase, product aldehyde is released, the substrate

® Abstract published in *Advance ACS Abstracts,* April 1, 1994.

(1) (a) Knowles, P. F.; Yadav, K. D. S. In *Copper Proteins and Copper Enzymes*; Lontie, R., Ed.; CRC Press: Boca Raton, FL, 1984; Vol. 2, pp 103–129. (b) Mondovi, B. *Structure and Function of Amine Oxidases*; Modovi, B., Ed.; CRC Press: Boca Raton, FL, 1985.

(2) van Iersel, J.; van der Meer, R. A.; Duine, J. A. *Eur. J. Biochem.* **1986**, *161*, 413–419.

(3) Dooley, D. M.; McIntire, W. S.; McGuirl, M. A.; Cote, C. E.; Bates, J. L. *J. Am. Chem. Soc.* **1990**, *112*, 2782–2789.

(4) Klinman, J. P.; Janes, S.; Hartmann, C. *Pharmacol. Res. Commun.* **1988**, *20*, 35–37.

(5) Janes, S. M.; Klinman, J. P. *Biochemistry* **1991**, *30*, 4599–4604.

(6) Janes, S. M.; Mu, D.; Wemmer, D.; Smith, A. J.; Kaur, S.; Maltby, D.; Burlingame, A. L.; Klinman, J. P. *Science* **1990**, *248*, 981–987.

(7) Dooley, D. M.; McGuirl, M. A.; Brown, D. E.; Turowski, P. N.; McIntire, W. S.; Knowles, P. F. *Nature* **1991**, *349*, 262–264.

(8) Janes, S. M.; Palcic, M. M.; Scaman, C. H.; Smith, A. J.; Brown, D. E.; Dooley, D. M.; Mure, M.; Klinman, J. P. *Biochemistry* **1992**, *31*, 12147–12154.

(9) Mu, D.; Janes, S. M.; Smith, A. J.; Brown, D. E.; Dooley, D. M.; Klinman, J. P. *J. Biol. Chem.* **1992**, *267*, 7979–7982.

(10) Davidson, V. L. *Principles and Applications of Quinoproteins*; Davidson, V. L., Ed.; Marcel Dekker, Inc.: New York, 1992.

(11) Stubbe, J. *Annu. Rev. Biochem.* **1989**, *58*, 257–285.

(12) Hoganson, C. W.; Babcock, G. T. *Biochemistry* **1992**, *31*, 11874–11880.

(13) (a) Olsson, B.; Olsson, J.; Pettersson, G. *Eur. J. Biochem.* **1976**, *71*, 375–382. (b) Olsson, B.; Olsson, J.; Pettersson, G. *Eur. J. Biochem.* **1978**, *87*, 1–8. (c) Ruis, F. X.; Knowles, P. F.; Pettersson, G. *Biochem. J.* **1984**, *220*, 767–772. (d) Farnum, M.; Palcic, M.; Klinman, J. P. *Biochemistry* **1986**, *25*, 1898–1904. (e) Olsson, B.; Olsson, J.; Pettersson, G. *Eur. J. Biochem.* **1976**, *64*, 327–331.

(14) Hartmann, C.; Klinman, J. P. *Biochemistry* **1991**, *30*, 4605–4611.

(15) Hartmann, C.; Klinman, J. P. *J. Biol. Chem.* **1987**, *262*, 962–965.

(16) Hartmann, C.; Brzovic, P.; Klinman, J. P. *Biochemistry* **1993**, *32*, 2234–2241.

(17) (a) Snell, E. E.; Di Mari, S. J. In *The Enzymes*; Boyer, P. D., Ed.; Academic Press: New York, 1970; pp 335–370. (b) Rodriguez, E. J.; Bruice, T. C. *J. Am. Chem. Soc.* **1989**, *111*, 7947–7956.

0002-7863/94/1516-4028$04.50/0

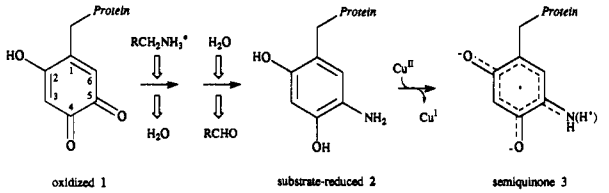

Figure 1. Depiction of reactions leading to formation of the topa-semiquinone intermediate in amine oxidase. The reductive phase and part of the oxidative phase of the overall amine oxidase catalytic cycle are indicated. Horizontal arrows represent the direction of the *in vivo* reaction. Vertical arrows represent addition/elimination reactions, with the indicated input and output species. The topa-quinone is depicted as the *ortho*-carbonyl tautomer. The positions of the oxygen and nitrogen substituents on the ring are at present unknown. The isomer shown is based on previous convention.[6,32] Protons that are hydrogen bonded to the semiquinone, as identified in this study, are shown in parentheses.

nitrogen atom remains bound to the enzyme, and the cofactor assumes a two-electron-reduced, hydroquinone form (**2**).[5,7,13a,14,16,18]

Insight into the subsequent, poorly understood oxidative steps of the reaction was recently gained from room-temperature CW-EPR studies of amine oxidase that were performed under anaerobic conditions to block completion of the reaction cycle: a paramagnetic, $g \sim 2$ topa-semiquinone/Cu^I state was revealed to be in temperature-dependent equilibrium with the substrate-reduced topa-hydroquinone/Cu^{II} state.[7] This equilibrium is established rapidly, at a catalytically competent rate.[19] These results strongly suggest that the semiquinone/Cu^I state is a *bona fide* intermediate along the native catalytic pathway and that the topa-aminohydroquinone acts as an electron-transfer donor to the Cu^{II} acceptor at the copper site. In addition, the CW-EPR spectra of the topa-semiquinone **3** in amine oxidase prepared by anaerobic reduction with ^{15}N- *versus* ^{14}N-labeled amine displayed a marked isotope effect on the EPR line shape.[3] This demonstrated that the unpaired spin was partially delocalized onto the substrate-derived nitrogen atom.[2,7] Subsequent electron spin echo envelope modulation (ESEEM) spectroscopic studies definitively demonstrated the formation of a covalent nitrogen–topa-semiquinone adduct and yielded ^{14}N hyperfine and nuclear quadrupole coupling parameters consistent with an imino-type nitrogen atom.[20] In the presence of dioxygen, a second electron transfer from the topa-semiquinone to the copper site would promote the release of product ammonia (under aerobic conditions, ammonia is released concomitant with H_2O_2)[13c,13e] and, thus, regeneration of the resting state of the enzyme.

In the present work, we characterize the hyperfine coupling of aqueous solvent-exchangeable ^1H and ^2H nuclei with the unpaired spin in the topa-semiquinone in bovine amine oxidase. This is done by comparing enzyme that had been substrate-reduced in ^1H_2O or in ^2H_2O buffer and stabilized in the semiquinone/Cu^I state for spectroscopic investigation at cryogenic temperatures by addition of the exogenous Cu^I-stabilizing ligand, cyanide.[2,7,20,21] The solvent comparison strategy is particularly illuminating in the case of the amine oxidase topa-semiquinone, because, as shown in Figure 1, there are three heteroatom centers capable of exchange. A combination of two high-resolution EPR techniques, the ESEEM technique of pulsed-EPR spectroscopy[22] and continuous wave–electron nuclear double resonance (CW-ENDOR),[23] is used selectively to characterize the hyperfine interactions from different classes of exchangeable nuclei. ^2H ESEEM is used to detect highly anisotropic coupling, owing to the inherent high sensitivity of the technique to low γ_N nuclei and to the diminished spectral width of the ^2H line shapes relative to their ^1H counterparts. In contrast, weak dipolar hyperfine couplings, such as those from hydrogen-bonded[24] ^2H nuclei, yield corresponding weak envelope modulation[25,26] and spectral features that are not resolved from the broad matrix ^2H feature. Proton CW-ENDOR is therefore chosen to characterize these couplings. The protonation states of the heteroatoms and detailed characterization of the electronic and nuclear structure at the nitrogen atom that are derived from the measured hyperfine parameters provide detailed insight into how the protein directs amine oxidation catalysis.

Materials and Methods

Protein Isolation and Preparation. Bovine amine oxidase was purified[6] and the reduced radical prepared[3] as described previously. Exchange against ^2H_2O buffer was carried out as described.[21] During this procedure, the sample was exposed to ^2H_2O for a total of 2 h. Samples in 0.1 M potassium phosphate buffer, pH 7.2, were concentrated by ultrafiltration and loaded into 4 mm o.d. quartz EPR tubes. The absolute spin concentrations of the samples in ^1H_2O and ^2H_2O buffer were determined to be 0.28 and 0.22 mM, respectively. ^2H_2O was purchased from Cambridge Isotope Laboratories.

Continuous Wave EPR Spectroscopy. CW-EPR spectra were obtained at X-band on a Bruker ER200D EPR spectrometer by using a Bruker TE102 EPR cavity. The external magnetic field strength was measured with a Bruker ER035M NMR gaussmeter, and the microwave frequency was measured with an EIP Microwave Model 25B frequency counter.

Continuous Wave ENDOR Spectroscopy. ENDOR measurements were performed by using the Bruker ER2OOD EPR spectrometer with the Bruker ER250 ENDOR/TRIPLE accessory and the Bruker ER250ENB ENDOR cavity. Radio-frequency power from a Wavetek 3000-446 signal generator was directed to an ENI 3100L amplifier and subsequently into a home-built coil assembly[27,28] that was terminated at 50 Ω. The cavity circuit remained matched at 50 ± 10 Ω in the radio-frequency range of 10–20 MHz.

ESEEM Spectroscopy. The home-built pulsed-EPR spectrometer used in this work has been described.[29] Reconstruction of envelope modulation that was lost in the dead time in two-pulse experiments (120 ns), or during the time interval $\tau + T_0$ in three-pulse experiments, was performed prior to Fourier transformation as described.[30]

Theoretical Simulations. Computer simulation of the ESEEM data was based on the density matrix treatment of Mims.[25,31] Simulations were run on Apple Macintosh II computers or on a DEC Vaxstation 4000. The experimental dead time was included in the time domain simulations, with the dead time reconstruction[30] performed prior to Fourier transformation as in the analysis of the experimental data.

The success of the ESEEM simulations was judged according to the match with the experimental three-pulse ESEEM spectra on the basis of the following constraints: (a) the magnetic field dependence of the line shape and frequency position at 0.3275, 0.3562, and 0.4202 T and

(18) Palcic, M.; Klinman, J. P. *Biochemistry* **1983**, *22*, 5957–5966.
(19) Turowski, P. N.; McGuirl, M. A.; Dooley, D. M. *J. Biol. Chem.* **1993**, *268*, 17660-17682.
(20) McCracken, J. L.; Peisach, J.; Cote, C. E.; McGuirl, M. A.; Dooley, D. M. *J. Am. Chem. Soc.* **1992**, *114*, 3715–3720.
(21) McCracken, J. L.; Peisach, J.; Dooley, D. M. *J. Am. Chem. Soc.* **1987**, *109*, 4064–4072.
(22) (a) Kevan, L.; Schwartz, R. N. *Time Domain Electron Spin Resonance*; John Wiley & Sons: New York, 1970. (b) Kevan, L.; Bowman, M. K. *Modern Pulsed and Continuous Wave Electron Spin Resonance*; John Wiley & Sons: New York, 1990. (c) Schweiger, A. *Angew. Chem., Int. Ed. Engl.* **1991**, *30*, 265–292.
(23) (a) Kevan, L.; Kispert, L. D. *Electron Spin Double Resonance Spectroscopy*; Wiley & Sons, New York, 1976. (b) Lubitz, W.; Babcock, G. T. *Trends Biochem. Sci.* **1987**, *12*, 96–100. (c) Bender, C. J.; Aisen, P. *Methods Enzymol.* **1993**, *227*, Part D, 190–231.
(24) (a) O'Malley, P. J.; Chandreshekar, T. K.; Babcock, G. T. In *Antennas and Pigments of Photosynthetic Bacteria*; Michel-Beyerle, M. E., Ed.; Springer-Verlag: Berlin, 1985; pp 385. (b) O'Malley, P. J.; Babcock, G. T. *J. Am. Chem. Soc.* **1986**, *108*, 3995–4001.
(25) Mims, W. B. *Phys. Rev. B* **1972**, *5*, 2409–2419.
(26) (a) Dooley, D. M.; McGuirl, M. A.; Peisach, J.; McCracken, J. *FEBS Lett.* **1987**, *214*, 274–278. (b) Finazzi-Agro, A.; Rinaldi, A.; Floris, G.; Rotilio, G. *FEBS Lett.* **1984**, *214*, 378–380.
(27) (a) Hurst, G.; Kraft, K.; Schultz, R.; Kreilick, R. *J. Magn. Reson.* **1982**, *49*, 159–160. (b) Bender, C. J.; Babcock, G. T. *Rev. Sci. Instrum.* **1992**, *63*, 3523–3524.
(28) Bender, C. J.; Sahlin, M.; Babcock, G. T.; Barry, B. A.; Chandrashekar, T. K.; Salowe, S. P.; Stubbe, J.; Lindstrom, B.; Petersson, L.; Ehrenberg, A.; Sjoberg, B.-M. *J. Am. Chem. Soc.* **1989**, *111*, 8076–8083.
(29) McCracken, J. L.; Shin, D.-H.; Dye, J. L. *Appl. Magn. Reson.* **1992**, *3*, 305–316.
(30) Mims, W. B. *J. Magn. Reson.* **1984**, *59*, 291–306.
(31) Mims, W. B. *Phys. Rev. B* **1972**, *6*, 3543–3545.

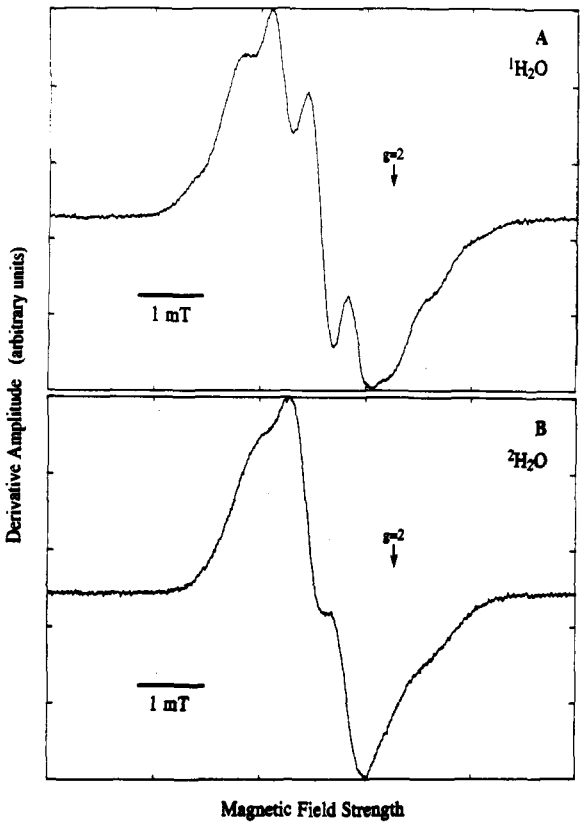

Figure 2. Continuous wave EPR spectra of bovine amine oxidase reduced anaerobically with benzylamine in the presence of 1 mM cyanide ion in ^1H_2O (A) and ^2H_2O (B) buffer. Conditions: microwave power, 10 μW; microwave frequency, 9.55 GHz; magnetic field modulation, 0.05 mT; modulation frequency, 100 kHz; temperature, 110 K. In the ESEEM studies, the frequency of the microwave pulse corresponds to the absorption maximum at the zero crossing of the EPR line.

(b) the τ suppression behavior. The deuterium nuclear quadrupole interaction did not significantly alter the appearance of the simulated ESEEM spectra. This is consistent with the large magnitudes of the hyperfine and nuclear Zeeman terms relative to the ^2H nuclear quadrupole coupling constant, $e^2qQ/4h$, of 0.05 MHz.[32]

Computation of the distance, B_0 orientation, and p-orbital shape dependence of the α-couplings and hydrogen-bonded couplings was performed by using Matlab programs on a Sun Sparcstation 2 or Macintosh II computers (B_0 is the laboratory magnetic field).

Results

Continuous Wave EPR Spectroscopy. Figure 2 shows CW-EPR spectra of bovine amine oxidase that had been reduced by benzylamine substrate in ^1H_2O and ^2H_2O buffer in the presence of cyanide ion. The EPR line shape of the enzyme in ^1H_2O buffer is comparable with that obtained previously for the enzyme from *Arthrobacter* P1,[3] porcine kidney,[26a] and lentil seedling.[26b] The comparable EPR spectra displayed by these enzymes indicate qualitatively that the structure of the topa-semiquinone in copper-containing amine oxidases from divergent sources is comparable. Figure 2 shows that the EPR line shape is altered dramatically by solvent exchange, which indicates a relatively strong magnetic interaction of one or more solvent-exchangeable protons with the unpaired electron spin. Further characterization of these and other exchange-sensitive hyperfine couplings by using CW-EPR spectroscopy is precluded by the extent of inhomogeneous line broadening.

ESEEM Spectroscopy: Characterization of Exchangeable ^2H Hyperfine Couplings. A. Spectral Extent. ESEEM spectroscopy of ^2H nuclei was used to resolve contributions to the strong, exchangeable hyperfine coupling. Figure 3A shows three-pulse

(32) Edmonds, D. T. *Phys. Lett. C* **1977**, *29*, 233–290.

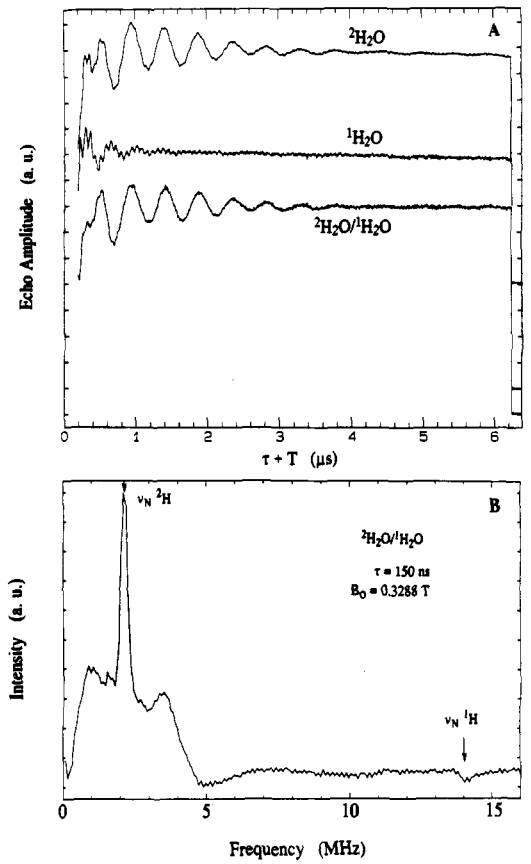

Figure 3. Stimulated-echo ESEEM of topa-semiquinone in bovine amine oxidase. The frequency of the pulsed microwave magnetic field in this and the following ESEEM measurements corresponds to the center of the EPR line shapes. (A) Envelope modulation from enzyme in ^2H_2O buffer (top) and ^1H_2O buffer (middle) and the ratio of the envelopes (bottom). (B) Fourier transformation of the divided envelope modulation. Experimental conditions: τ, 150 ns; initial T (T_0), 40 ns; microwave frequency, 9.13 GHz; magnetic field strength, 0.3288 T; microwave pulse power, 40 W (20 ns fwhm); pulse sequence repetition rate, 10 Hz; 10 events averaged per time point; temperature, 4.2 K.

envelope modulation data collected at a τ value of 150 ns under identical spectrometer conditions for enzyme in ^2H_2O and ^1H_2O buffer. Division of the envelopes[33] attenuates modulation components from nonexchangeable nuclei, in particular, those arising from coupling to the substrate-derived ^{14}N nucleus,[20] and therefore enhances modulation contributions from ^2H nuclei. The Fourier transformation of the divided envelope modulation, presented in Figure 3B, displays the hyperfine frequencies contributing to the envelope modulation. The position of the narrow line at the ^2H Larmor frequency (ν_N) of 2.2 MHz indicates that it arises from exchangeable nuclei that are coupled to the electron spin through weak magnetic dipolar interactions. As expected, a corresponding negative feature, representing the ^1H nuclei replaced by ^2H, is observed at the proton Larmor frequency of 14.1 MHz. The weaker intensity of the ^1H matrix line results from the suppression effect[31] that will be described below. The ESEEM spectrum in Figure 3B also shows modulation components with frequencies extending from about 0.3 to 4.1 MHz. The symmetric disposition of these features with respect to the ^2H matrix line suggests that they arise from relatively strong hyperfine interaction of the unpaired electron with one or more exchangeable ^2H nuclei.

B. Microwave Frequency/Magnetic Field Dependence. The tandem microwave transmitter frequency and external magnetic

(33) (a) Rowan, L. G.; Hahn, E. L.; Mims, W. B. *Phys. Rev.* **1965**, *137*, A61–A71. (b) Mims, W. B.; Peisach, J. In *Advanced EPR: Applications in Biology and Biochemistry*; Hoff, A. J., Ed.; Elsevier, New York, 1989; pp 1–57.

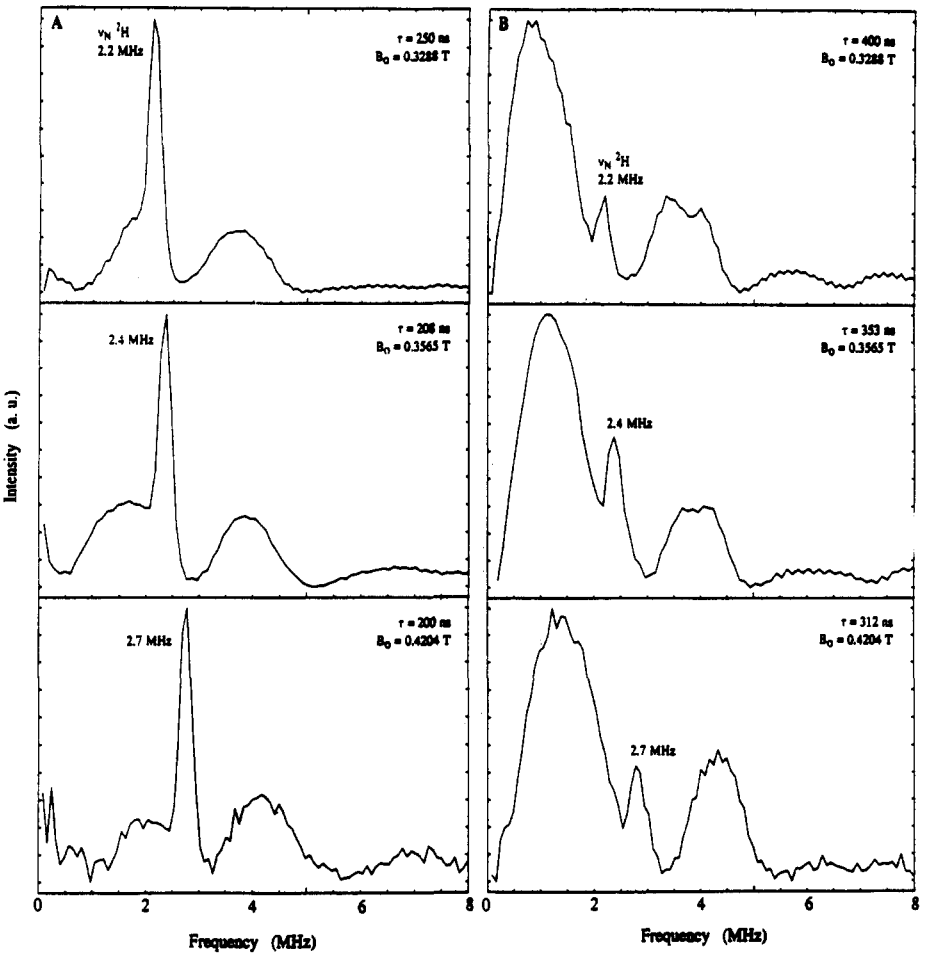

Figure 4. Three-pulse ESEEM ratio spectra of substrate-reduced bovine amine oxidase in ^2H_2O and ^1H_2O buffer as a function of τ and magnetic field strength. The magnetic field strength increases from top to bottom in each colum, as indicated. The τ values are scaled so that the nuclear precession periods correspond to the values of 250 ns (column A) or 400 ns (column B) at 0.3288 G. The microwave frequencies used at 0.3288, 0.3565, and 0.4204 T were 9.13, 9.94, and 11.71 GHz, respectively. The microwave pulse powers used at 0.3565 and 0.4204 T were 40 and 200 W, respectively. All other conditions as described in the legend to Figure 3.

field strength dependence of the line positions in the ESEEM spectrum are used to identify the type of coupled nucleus[34] and to resolve overlapping features from different types of nuclei. Figure 4 shows that changing the magnetic field strength shifts the broad line shape *en bloc* to an extent that corresponds to the shift in the free ^{2}H Larmor frequency. The same magnetic field change would lead to frequency position shifts of 0.3 and 4.6 MHz for any features arising from ^{14}N and ^{1}H nuclei, respectively. Therefore, we conclude that ^{2}H hyperfine interactions give rise to the broad spectral features. Distortion of these features by overlapping ^{14}N or ^{1}H contributions is not significant.

C. τ-Suppression Effects. In order to determine whether all or part of the broad features in Figures 3 and 4 arise from hyperfine splitting of the $m_s = +^1/_2$ (hyperfine frequency component, $\nu_{\alpha,ij}$, where i and j refer to nuclear sublevels) and $m_s = -^1/_2$ ($\nu_{\beta,ij}$) electron spin manifolds by a particular, chemical class of ^{2}H nucleus, the τ suppression effect[31] was employed. When the value of τ is set equal to an integral number of cycles of one nuclear frequency, say $\nu_{\beta,ij}$, the contribution of the conjugate frequency component $\nu_{\alpha,ij}$ to the envelope modulation is suppressed. At half-integral values of $(\nu_{\beta,ij})^{-1}$, the envelope modulation due to ν_α is relatively enhanced. Parts A and B of Figure 4 show that the portion of the broad feature at $\nu < \nu_N$ is suppressed at τ = 250 ns and relatively enhanced at τ = 400 ns. Suppression and enhancement effects are also observed for all regions of the broad features that are separated symmetrically from the ^{2}H matrix line in data collected using the conventional three-pulse sequence at τ values from 130 to 500 ns. Therefore, the two broad envelopes correspond to hyperfine splitting of the $m_s = +^1/_2$ and $m_s = -^1/_2$ electron spin manifolds by at least one chemical class of ^{2}H nucleus. The observed ^{2}H hyperfine coupling thus obeys the condition $A/2 < \nu_N$, where A denotes the powder orientation-dependent hyperfine coupling.

D. ESEEM at Long τ Values. Although the τ suppression effect is useful for assigning resonances, a disadvantage is that the effect can create regions of zero intensity, or "blind spots", that distort the line shape.[31,35] To relieve suppression of higher frequency components of the line shape positioned at $\nu > \nu_N$, values of $\tau > 500$ ns are necessary.[36] The large effective dead time that accompanies long τ values is reduced by integrating the stimulated echo intensity for $T < \tau$, as well as for $T > \tau$ as in a conventional three-pulse experiment, by using the microwave pulse-swapping technique.[35,37] As shown in Figure 5A, envelope division is used to remedy the background decay-induced discontinuities in the individual time domains that occur at the eclipse of the second and third 90° microwave pulses when pulse swapping is employed.[36] The resulting ESEEM spectrum in Figure 5B exhibits intensity buildup in the high-frequency feature beginning at ~2.8 MHz that extends to 4.1 MHz. The slightly shorter phase memory time of the enzyme sample in ^2H_2O produces a downward trend in the amplitude of the divided echo envelope at $\tau + T < \tau$, which introduces an artifactual low-

(34) Lai, A.; Flanagan, H. L.; Singel, D. J. *J. Chem. Phys.* **1988**, *89*, 7161–7166.

(35) Fauth, J. M.; Schweiger, A.; Braunschweiler, L.; Forrer, J.; Ernst, R. R. *J. Magn. Reson.* **1986**, *66*, 74–86.

(36) Warncke, K.; McCracken, J. **1994** *J. Chem. Phys.*, submitted.

(37) Fauth, J. M.; Schweiger, A.; Ernst, R. R. *J. Magn. Reson.* **1989**, *81*, 262–274.

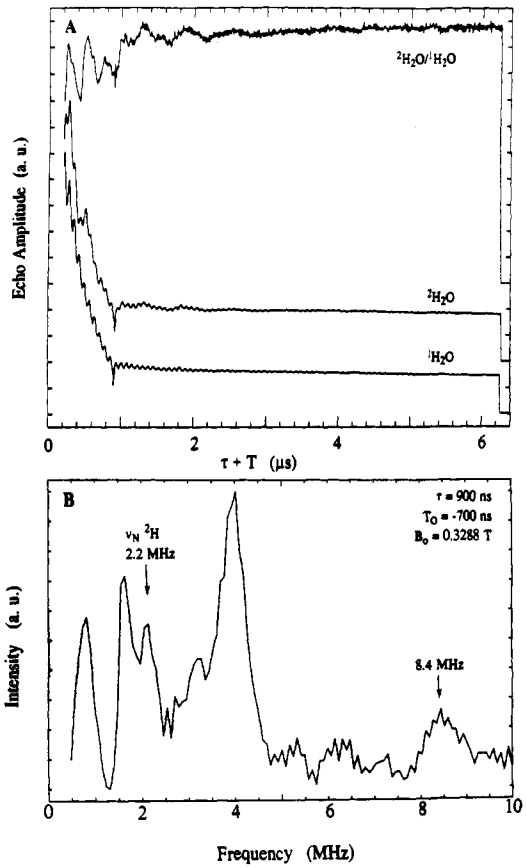

Figure 5. Three-pulse ESEEM spectra of substrate-reduced bovine amine oxidase in ^2H_2O and ^1H_2O buffer obtained using the pulse-swapping method. Panel A shows the envelope modulation for individual samples in ^2H_2O and ^1H_2O (bottom) and the envelope-divided time domain (top). Panel B shows the Fourier transformation of the envelope-divided envelope modulation. Experimental conditions: τ, 900 ns; T_0, -700 ns; microwave frequency, 9.13 GHz; magnetic field strength, 0.3288 T; microwave pulse power, 40 W (20 ns fwhm); pulse sequence repetition rate, 10 Hz; 10 events averaged per time point; temperature, 4.2 K.

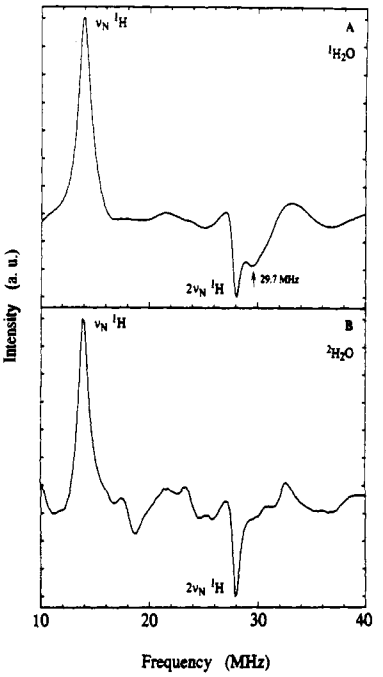

Figure 6. Two-pulse ESEEM spectrum of bovine amine oxidase. (A) ^1H_2O buffer; (B) ^2H_2O buffer. Experimental conditions as described in Figure 2. The initial value of τ was 120 ns. The ordinate scale of the ^2H_2O spectrum is increased by a factor of 1.4 relative to that of the ^1H_2O spectrum.

frequency feature of negative phase in the frequency spectrum shown in Figure 5B. The resulting descent in the baseline as zero frequency is approached diminishes the amplitude of the low-frequency features (<2 MHz) and obscures the spectral region below 0.5 MHz. Nevertheless, two intensity maxima are resolved in the lower frequency feature at 0.8 and 1.6 MHz. In addition, a new feature that is not observed in conventional three-pulse data appears centered at 8.4 MHz, and weak intensity appears in the region around 6 MHz. These features are in the region expected for a ^2H $\Delta m_I = \pm 2$, or "double quantum", transition corresponding to the feature at ~2.8–4.1 MHz.

The pulse-swapping and conventional three-pulse measurements reveal a line shape extending over the frequency ranges 0.3–1.6 and 2.7–4.1 MHz (microwave frequency, 9.12 GHz; magnetic field strength, 0.3250 T) that is shaped by distinct τ-dependent suppression effects. The τ-suppression and magnetic field strength dependence of the line shape provide stringent constraints on theoretical simulations of the spectra that are necessary to determine accurately the principal hyperfine tensor values.[36,38]

ESEEM Characterization of Exchangeable ^1H Hyperfine Couplings. ESEEM spectra obtained using the two-pulse, Hahn echo sequence provide direct evidence for exchangeable ^1H in the spectral region of the ^1H $\nu_\alpha + \nu_\beta$, or sum combination, line. Lines arising from sums and differences of the fundamental frequencies, ν_α and ν_β, are absent in three-pulse spectra but can be observed in two-pulse spectra and are marked by a negative phase. As shown by the spectrum for substrate-reduced amine oxidase in ^1H_2O buffer presented in Figure 6A, a broad feature appears with a minimum shifted by +1.7 MHz from the ^1H Larmor sum frequency at $2\nu_N$. This feature is absent in the ^2H_2O sample spectrum shown in Figure 6B. The additional negative and positive features in the spectrum in Figure 6B *versus* 6A that are offset from the ^1H $\nu_\alpha + \nu_\beta$ line represent second-order terms in the modulation that arise from combinations of the relatively weak ^1H modulation components with the extremely strong ^2H modulation. Theoretical treatments have shown that features in the $\nu_\alpha + \nu_\beta$ line that are shifted from $2\nu_N$ arise from hyperfine interactions that include a strong dipolar contribution.[42] The two-pulse results therefore provide direct evidence for a solvent-exchangeable ^1H nucleus with a strong dipolar component of interaction with unpaired spin density on the topa-semiquinone.

CW-ENDOR Spectroscopy. Exchangeable ^1H couplings are identified by their dissappearance from the ENDOR spectrum in the region of the proton Larmor frequency upon exchange with ^2H_2O.[23] After ^2H_2O exchange, the corresponding deuterium hyperfine transitions appear near to the ^2H Larmor frequency and are not observed in the radio-frequency range examined here. Figure 7 shows proton ENDOR spectra, obtained in the absorption derivative mode, of the amine oxidase samples in the radio-

(38) In CW-ENDOR spectra, intensity buildup is observed at positions of the extrema of the anisotropic hyperfine coupling interaction, which are established by the sum of half the principal values of the hyperfine tensor and the nuclear Zeeman frequency.[23a] However, this is not true for ESEEM spectra, because the relative contribution of spectral components of the anisotropically broadened line is influenced not only by blind spots[31,33b] but also by two other factors.[39] First, intensity arising from spin packets that would be at the extremes of the $m_s = {}^1/_2$ and $-{}^1/_2$ powder pattern ENDOR lines is decreased because the ESEEM transition probabilities approach zero for orientations of the spin system such that the magnetic field is along the principal axes.[40] Second, loss of anisotropic information in the instrument dead time can diminish intensity in the central region of broad ESEEM lines.[41] Simulations show that the effect of dead time on the relatively narrow ^2H line shapes examined here is negligible.

(39) Reijerse, E. J.; Keijers, C. P. *J. Magn. Reson.* **1987**, *71*, 83–96.
(40) De Groot, A.; Evelo, R.; Hoff, A. J. *J. Magn. Reson.* **1986**, *66*, 331–343.
(41) Astashkin, A. V.; Dikanov, S. A.; Tsvetkov, Yu. D. *Chem. Phys. Lett.* **1987**, *136*, 204–208.
(42) (a) Dikanov, S. A.; Astashkin, A. V. In *Advanced EPR: Applications in Biology and Biochemistry*; Hoff, A. J., Ed.; Elsevier: New York, 1989; pp 59–117. (b) Reijerse, E. J.; Dikanov, S. A. *J. Chem. Phys.* **1991**, *95*, 836–845.

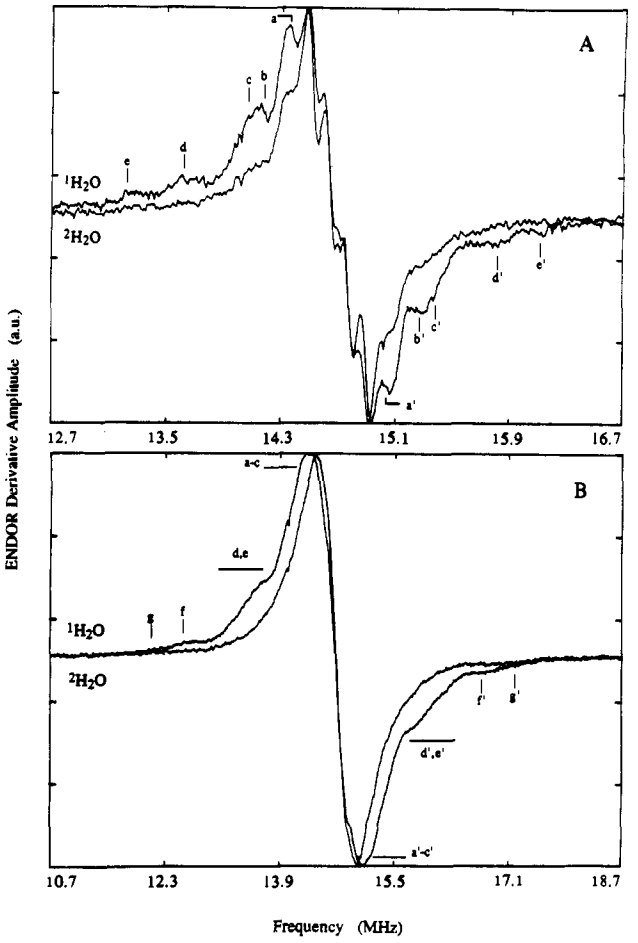

Figure 7. Proton CW-ENDOR spectra of substrate-reduced methylamine oxidase in ^2H_2O and ^1H_2O buffer. (A) High-resolution spectrum. Experimental conditions: microwave power, 1 mW; magnetic field strength, 0.3448 T; radio-frequency power, 50 W; FM, 20 kHz; temperature, 137 K. (B) High-power and FM spectrum. Conditions: same as for part A except rf power, 100 W; FM, 150 kHz; temperature, 113 K. The ^1H Larmor frequency is 14.69 MHz and corresponds to the zero crossing of the derivative line shape. The spectra were taken at the maximum EPR absorption, equivalent to the zero crossing of the EPR line shapes shown in Figure 2. Note that the horizontal frequency scale for panels A and B is different. The spectra were obtained with the same samples used in the ESEEM studies. Positions of turning points are indicated by lower case letters.

frequency region of 10–20 MHz that includes the ^1H ν_N value of 14.69 MHz. Figure 7A shows data collected under conditions of relatively low radio frequency power and frequency modulation that enhance the spectral resolution at the expense of signal amplitude. Five pairs of transitions (designated a,a′–e,e′ in Figure 7A) that are disposed symmetrically about the free proton frequency are clearly observed in the ^1H_2O spectrum that display zero or severely reduced intensity in the ^2H_2O sample spectrum. These pairs of features thus represent components of the ν_α and ν_β hyperfine transitions of solvent-exchangeable ^1H nuclei. The values of the hyperfine couplings, obtained from the frequency difference between the pairs of features, are listed in Table 1. In the ^2H_2O-exchanged sample, the small amplitude contributions at radio frequencies identical to those for the a,a′–c,c′ exchangeable couplings probably arise from residual amounts of ^1H_2O in the ^2H_2O sample or incomplete exchange. For example, residual features from exchangeable ^1H nuclei have been observed following ^2H_2O exchange,[24b] as well as in chemical ^2H-substitution experiments where the ^2H isotope enrichment was >98%.[43]

(43) (a) Rist, G. H.; Hyde, J. S.; Vänngård, T. *Proc. Natl. Acad. Sci.* **1970**, *67*, 79–86. (b) Fritz, J.; Mueller, F.; Mayhew, S. G. *Helv. Chim. Acta* **1973**, *56*, 2250–2254.

Table 1. Aqueous Solvent Exchangeable Hyperfine Couplings (hfc) of ^1H Nuclei to the Unpaired Electron Spin Density in the Topa-semiquinone As Determined by CW-ENDOR

designation	hfc (MHz)	assignment
a–a′	0.7	$A_\perp$, O_B···^1H
b–b′	1.1	$A_\perp$, O_A···^1H
c–c′	1.3	$A_\parallel$, O_B···^1H
d–d′	2.1	$A_\parallel$, O_A···^1H
e–e′	2.9	A_z, N···^1H
f–f′	4.2	A_x, N···^1H
g–g′	6.0	A_y, N···^1H

Intensity from nonexchangeable ^1H nuclei underlies the exchangeable features in Figure 7.

Hyperfine transitions that are not observed under the low signal-to-noise spectrometer conditions of Figure 7A are revealed at higher radio frequency power and modulation at the expense of spectral resolution, as shown in Figure 7B. Figure 7B shows two additional pairs of exchangeable features, f,f′ and g,g′. The hyperfine coupling values are presented in Table 1.

Discussion

Exchangeable Strong $^2H/^1H$ Interaction. A. Characterization of the Strong Hyperfine Interaction. The relatively broad line widths in the ^2H ESEEM spectra are most simply interpreted as arising from magnetic interaction of the unpaired electron with a single chemical class of ^2H nucleus that is characterized by a hyperfine tensor of rhombic symmetry. In initial simulations of the three-pulse ^2H ESEEM spectra performed with a rhombic hyperfine tensor, we found good agreement with the experimental line shape and frequency positions. No additional interactions with magnetically distinct ^2H nuclei were necessary to reconstruct the data. During progress toward convergence of the simulations, the degree of anisotropy in the rhombic ^2H tensor was found to be substantial enough that it would lead to a splitting of the $\nu_\alpha + \nu_\beta$ line of the corresponding ^1H nucleus from $2\nu_N$ in two-pulse ESEEM spectra. This, in conjunction with the requirement for only one chemical type of strongly coupled ^2H nucleus, indicates that the splitting of the ^1H sum combination line and the ^2H features originate from interaction of the unpaired spin density with the same exchangeable position on the topa-semiquinone. Reproduction of the splitting of the ^1H combination line was therefore included as an additional simulation constraint. The incorporation of the ^1H sum combination line splitting constraint assisted in targeting the value of the smallest magnitude principal component. This is because of the strong influence of the tensor rhombicity[44] on the shape and frequency position of the $\nu_\alpha + \nu_\beta$ feature.[42] The large number of constraints on the simulations allowed determination of all three principal tensor components to uncertainties of ±0.1 MHz.

Representative simulated three-pulse ^2H ESEEM spectra that correspond to the experimental spectra in Figures 4 and 5 are presented in Figure 8A–C. The principal values of the hyperfine tensor obtained from simulations of the experimental spectra at the different τ and magnetic field strength values are listed in Table 2. Figure 8D shows a frequency histogram computed from these principal values that includes all possible hyperfine frequencies weighted only by the distribution of random molecular orientations (that is, an "ideal" ENDOR absorption spectrum). Differences among the frequency histogram and the simulated and observed ESEEM spectra demonstrate the influence of the

(44) The rhombicity, denoted as "δ", is defined as $\delta = (A_{dip,x} - A_{dip,y})/A_{dip,z}$, when z is along the line connecting electron and nucleus and x and y are perpendicular to this axis.[42b] The dipolar tensor components, $A_{dip,i}$, are described later in the text. Using an analytical expression for the combination line splitting[42b] and the parameters in Table 2, we find that the feature at $2\nu_N$ + 1.7 MHz represents primarily the contribution of spin systems in the powder that have B_0 oriented along the y-axis. Contributions from the $B_0 \| x$ orientation are predicted at $>2\nu_N$ + 1.7 MHz but are not clearly observed at the experimental signal-to-noise level and resolution of the two-pulse experiment.

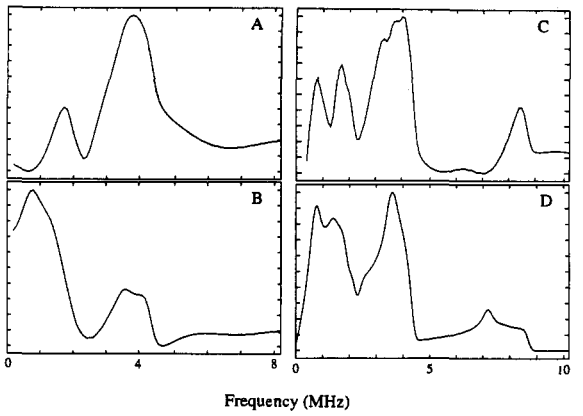

Figure 8. Simulations of three-pulse ESEEM spectra from the strongly coupled ^2H nucleus. These simulated spectra correspond to the experimental conditions for the spectra presented in Figures 4 (top panels) and 5B. Nuclei coupled to the unpaired spin through weak dipolar interactions that give rise to intensity near the ^2H Larmor frequency in the experimental spectra are not included in the simulations. (A) τ = 250 ns. (B) τ = 400 ns. (C) τ = 900 ns. Simulation parameters: g_n, 0.8574; magnetic field strength, 0.3288 T; initial value of T, 40 ns for τ = 250 and 400 ns and −700 ns for τ = 900 ns; principal values of the hyperfine tensor, A_z = −2.9, A_x = −4.4, A_y = −0.2 MHz; ^2H nuclear quadrupole coupling parameters, $e^2qQ/4h$ = 0.05 MHz; asymmetry parameter, 0.1. (D) ENDOR frequency histogram. Simulation parameters: g_n, 0.8574; magnetic field strength, 0.3288 T; A_z = −2.9, A_x = −4.4, A_y = −0.2 MHz; ^2H nuclear quadrupole coupling parameters, $e^2qQ/4h$ = 0.05 MHz; asymmetry parameter, 0.1. An isotropic electronic g-factor was assumed in all simulations.

orientation-dependent envelope modulation depth and τ-suppression on the appearance of the ESEEM line shapes.[39] The pulse-swapped ESEEM spectrum most closely approximates the frequency histogram. This is because the long τ value relieves the suppression of the higher frequency portion of the line shape by the conjugate low frequency components, especially those near zero frequency. In particular, the $\Delta m_I = \pm 2$ transitions, which have not previously been reported in ^2H ESEEM studies, are partially revealed. Strong $\Delta m_I = \pm 2$ transition intensity is observed in the spectrum shown in Figure 5B around the maximum at 8.4 MHz, and weaker intensity is observed in the region around 6.3 MHz. Both of these features are reproduced in the ESEEM simulation in Figure 8C and correspond clearly to regions of the double-quantum intensity observed in the frequency histogram of Figure 8D. The amplitude and spectral extent of the double-quantum feature are strongly dependent on the large anisotropy of the tensor.[36] Observation of strong intensity at the double-quantum frequencies therefore provides support for attributing the ^2H ESEEM line shape to coupling with a single ^2H nucleus characterized by a highly anisotropic hyperfine tensor.

The rhombicity of the hyperfine tensor indicates a strong magnetic interaction expected for a covalently attached proton α to an atom that has unpaired electron spin density localized in a p-orbital. On the basis of previous theoretical and experimental characterizations of α-proton couplings, the principal values are all taken to be negative in sign.[45] Thus, the value of the isotropic coupling (A_{iso}) for the ^2H (^1H) nucleus is assumed to be −2.5 (−16.3) MHz. Values for A_{iso} and the dipolar components of the coupling ($A_{dip,i}$) are also presented in Table 2. Chart 1 shows schematically the relation between the hyperfine tensor axes and the molecular structure that we have adopted.

B. Number of Equivalent, Strongly Coupled ^2H Nuclei. Multiple, magnetically equivalent nuclei are revealed in ESEEM spectra by features at combinations of the fundamental ν_α and ν_β frequencies.[33b,46] Despite the observed strong ^2H modulation, no lines at combinations of the fundamentals are displayed in two- or three-pulse ESEEM spectra. In addition, simulation of ESEEM time domain data using two equivalent coupled nuclei with hyperfine parameters as in Table 2 generates modulation depths that are twice as large as those observed. We conclude that the strong coupling arises from a single ^2H nucleus.

C. Influence of the Strong, Exchangeable Coupling on the CW-EPR Spectrum. The relatively large value of A_{iso} and high anisotropy of the strong exchangeable coupling indicate that this nucleus is primarily responsible for the dramatic influence of solvent exchange on the CW-EPR line shape shown in Figure 2. Preliminary reconstructions of the EPR spectrum indicate that the large A_{iso} value for the strong ^1H coupling is essential for reproducing the width of the line. Quantitative analysis of the EPR line shape changes is complicated by the large anisotropy of both the exchangeable ^1H and ^{14}N interactions, as well as the g-anisotropy and the as yet unquantitated contributions from nonexchangeable ^1H nuclei. A thorough treatment of the CW-EPR spectrum will thus be presented following characterization of nonexchangeable hyperfine couplings (K.W., G.T.B., D.M.D., M.A.M., and J.M. Manuscript in preparation).

D. Position of the Strongly Coupled Nucleus on Topa-semiquinone. Candidates for the atom adjacent to the exchangeable α-type hydrogen are the three exchange-labile heteroatoms: the two quinonoid oxygens and the substrate-derived nitrogen. In addition, NMR studies have shown that slow $^2H/^1H$ exchange occurs at a proposed enolinic ring carbon atom in the fully solvent accessible phenylhydrazone adduct of topa-quinone released following proteolytic digestion of bovine serum amine oxidase.[6] However, a hyperfine coupling with a ring-bound α-proton of the strength that we observe is inconsistent with the generally low p_π-spin density on the ring carbon atoms in radicals substituted with multiple heteroatoms[47] and, specifically, the small magnitude of A_{iso} values (<|2.5| MHz) for the two ring α-^1H nuclei in dihydroxymethylaniline radicals, which model the topa-semiquinone.[48] It is reasonable to assume that there is at least one covalently bound proton on the nitrogen atom. This is not a necessary condition for the two oxygen atoms that, in the semiquinone state, have relatively weak pK_a values in the range 4–6 and are thus readily ionizable.[49] From these considerations, we assign the strong, exchangeable hyperfine interaction to a hydrogen nucleus that is attached covalently to the substrate-derived nitrogen atom.

Evidence for nitrogen as the adjacent atom is provided by the comparable values for the unpaired spin density on the nitrogen (ρ_N) that are estimated from the ^{14}N dipolar hyperfine coupling determined previously in the *Arthrobacter* enzyme (9 MHz)[20] and the A_{iso} value for the N–H interaction that we report here. The value of A_{iso} is chosen because it is unlikely to be influenced by hyperfine interactions with unpaired spin density localized on neighbor atoms, as expected for the dipolar tensor components. A normalized dipolar coupling for the nitrogen nucleus–p-electron interaction of 47.8 MHz[45b] yields an estimated ρ_N of 0.19. A range of McConnell Q^H_{NH} values for the isotropic α-^2H–N interaction of −11.1 to −10.3 MHz[50] provides estimated values for ρ_N of 0.23–0.25. The reasonable agreement between these two independently determined ρ_N values supports the assignment of nitrogen as the adjacent atom.

E. Comparison of the Observed and Estimated Dipolar Hyperfine Coupling Tensors. The values of the observed dipolar tensor components deviate significantly from values estimated

(45) (a) Carrington, A.; McLachlan, A. D. *Introduction to Magnetic Resonance*; Chapman & Hall: New York, 1980. (b) Wertz, J. E.; Bolton, J. R. *Electron Spin Resonance*; Chapman & Hall: New York, 1986.
(46) Mims, W. B.; Peisach, J. *J. Chem. Phys.* **1978**, *69*, 4921–4930.
(47) (a) Rieger, P. H.; Fraenkel, G. K. *J. Chem. Phys.* **1962**, *37*, 2811–2831. (b) Rieger, P. H.; Fraenkel, G. K. *J. Chem. Phys.* **1963**, *39*, 609–629.
(48) Dixon, W. T.; Hoyle, P. M.; Murphy, D. *J. Chem. Soc., Faraday Trans. 2* **1978**, *74*, 2027–2034.
(49) Swallow, A. J. In *Function of Quinones in Energy Conserving Systems*; Trumpower, B. L., Ed.; Academic Press: New York, 1982; pp 59–72.
(50) Gordy, W. In *Techniques of Chemistry, Volume XV: Theory and Applications of Electron Spin Resonance*; West, W., Ed.; Wiley & Sons: New York, 1980.

Table 2. Principal Hyperfine Tensor, Isotropic Hyperfine, and Dipolar Hyperfine Coupling Values for Aqueous Solvent Exchangeable Nuclei That Are Coupled Magnetically to Unpaired Spin Density in the Topa-semiquinone[a]

assignment	A_x	A_y	A_z	A_{iso}	$A_{dip,x}$	$A_{dip,y}$	$A_{dip,z}$
			Strong α-Interactions				
N–^{2}H	–4.4	–0.2	–2.9	–2.5	2.3	–1.9	–0.4
N–^{1}H	–28.6	–1.3	–18.9	–16.3	15.0	–12.4	–2.6
			Hydrogen-Bonded Interactions				
O_A···^{1}H	–1.1	2.1	–1.1	0	–1.1	2.1	–1.1
O_B···^{1}H	–0.7	1.3	–0.7	0	–0.7	1.3	–0.7
N···^{1}H	–4.2	6.0	–2.9	–0.4	–3.8	6.4	–2.5

[a] All values are given in units of MHz.

Chart 1

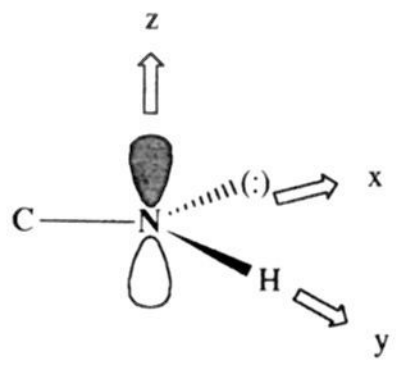

by using a simple physical model for the α-H–N interaction.[50] The model assumes a coplanar ring C–N–H system, as depicted in Chart 1, a standard N–H bond length of R = 1.01 Å, and an empirically derived value of 0.68 Å for the effective distance (R_p) between the nucleus and the unpaired electron along the direction of the nitrogen p_π-orbital axis.[50] The computed ^{2}H dipolar tensor is [–1.6, 1.7, –0.1] MHz. Comparison with the observed dipolar tensor in Table 2 indicates an excess dipolar coupling with components of [–0.3, 0.6, –0.3] MHz.

A possible source of the dipolar tensor distortion is hyperfine fields induced by unpaired spin density located on near-neighbor atoms. For example, next-neighbor interactions make significant contributions to α-H couplings in semiquinone and tyrosyl radicals.[24b,28] However, the two closest atomic centers where unpaired spin density might reside, the ring carbon atom to which the nitrogen is bonded (spin density ρ_C) and a possible *ortho*-substituted oxygen atom (ρ_O) (see Figure 1), are >2 Å from the N–H proton. The dipolar interactions would therefore be expected to be weak owing to the inverse third power dependence on distance. Further, the geometry of these interactions dictates that the influence of the hyperfine field emanating from the ring carbon atom or an *ortho*-substituted oxygen atom on $A_{dip,x}$ (in the N–H principal axis system) is 0.2(ρ_C) MHz or 1.6(ρ_O) MHz, respectively.[51] These effects are inconsistent with the magnitude and sign of the observed excess dipolar coupling along the principal x-axis of –0.3 MHz. Therefore, although near-neighbor nuclei exert small effects on the observed N–H dipolar coupling, this model cannot account for the bulk of the excess dipolar coupling.

Distortion of the dipolar tensor can be most simply accounted for by assuming that the nitrogen p_π-orbital containing the unpaired spin density in the topa-semiquinone is contracted relative to the 2p-orbital of a neutral nitrogen atom. Contraction of the p-orbital equivalent to a 10% decrease in the value of R_p (that is, to 0.61 Å) reduces the difference between calculated and measured dipolar coupling to roughly the level of uncertainty in the data ([0.1, 0.2, 0] MHz). Changes in screening of the effective nuclear charge that influences the spatial distribution of unpaired electron spin density in the p_π-orbital have been proposed previously to perturb hyperfine interactions with the nucleus and surrounding paramagnetic centers.[50,53] A crude upper limit on the extent of p-orbital contraction for a unit increase in nuclear charge of 14% is calculated from the average p-electron–nucleus distances obtained from the atom anisotropic hyperfine coupling values for interactions of a valence p-electron with ^{14}N and ^{17}O.[45b] These considerations suggest that the screening of the unpaired electron is reduced, and hence the effective nuclear charge enhanced, in the substrate-derived nitrogen atom of the topa-semiquinone relative to a neutral nitrogen atom.

F. Absence of Deuteroxyl ^{2}H Couplings. There is no evidence in the ^{2}H ESEEM spectra for exchangeable strong α-type couplings of deuteroxyl deuterons that might be covalently bonded to the topa-semiquinone oxygen atoms. Theoretical simulations were performed by using the R, R_p, and McConnell Q values for the covalent N–H interaction to estimate roughly the covalent O–H hyperfine coupling tensor for variable oxygen atom spin density (ρ_O). ESEEM simulations incorporating both the ^{2}H–N and the estimated ^{2}H–O couplings indicated that observable changes in the envelope modulation depths and frequency spectra from those observed for the ^{2}H–N interaction alone would be apparent for $\rho_O > 0.15$. Reported ρ_O values in semiquinones, obtained from molecular orbital calculations and companion EPR and ENDOR studies, are in the range 0.2–0.3.[54,55] Therefore, we propose that the oxygen atoms in the topa-semiquinone are deprotonated. Forthcoming efforts to simulate the CW-EPR spectra of the amine oxidase in the semiquinone/Cu^I state will provide a stringent check on the verity of this proposal.

Hydrogen-Bonded Proton Couplings. A. Assignment of the Hyperfine Couplings. Solvent-exchangeable, moderately strong ($\sim 1 \leq |A|/2 \leq \sim 8$ MHz) hyperfine couplings observed in the ^{1}H ENDOR spectra of heteroatom-containing organic π-radicals are considered to arise from protons involved in hydrogen bonds to the heteroatoms.[23a,24,28] Seven pairs of exchangeable hyperfine couplings are observed in the ENDOR spectra of amine oxidase shown in Figure 7. We assume that these exchangeable hyperfine couplings represent the interaction of hydrogen-bonded protons with the three heteroatom substituents on the topa-semiquinone.

B. Hydrogen Bond Interaction with the Substrate-Derived Nitrogen Atom. An approximate sp^2-hybridization of the nitrogen atom is indicated by its nuclear quadrupole coupling constant[20,56]

(51) The influences of the hyperfine fields from unpaired spin density located at the ring carbon atom (R = 2.0 Å, R_p = 0.7 Å) and a possible *ortho*-substituted oxygen atom (R = 2.4 Å, R_p = 0; values of R_p for oxygen have not been reported) on the principal values of the N–H dipolar tensor, defined along the molecular axes as depicted in Scheme 1, are calculated to be ρ_C[+0.2, 1.0, –0.9] MHz and ρ_O[1.6, –0.6, –0.8] MHz, respectively. The calculations are based on standard bond lengths and angles[52] and the assumption that all atoms lie in the plane of the topa-semiquinone ring.

(52) Sandorfy, C. In *The Chemistry of the Carbon–Nitrogen Double Bond*; Patai, S., Ed.; Wiley & Sons: London, 1970.

(53) (a) Karplus, M.; Pople, J. A. *J. Chem. Phys.* **1963**, *38*, 2803. (b) Bolton, J. R. *J. Chem. Phys.* **1965**, *43*, 309–310.

(54) (a) Gendell, J.; Freed, J. H.; Fraenkel, G. K. *J. Chem. Phys.* **1962**, *37*, 2832–2841. (b) Vincow, G. *J. Chem. Phys.* **1963**, *38*, 917–919.

(55) Feher, G.; Isaacson, R. A.; Okamura, M. Y.; Lubitz, W. In *Antennas and Pigments of Photosynthetic Bacteria*; Michel-Beyerle, M. E., Ed.; Springer-Verlag: Berlin, 1985; pp 174–189.

(56) The electric field gradient at the ^{14}N nucleus is created predominantly by the nonbonding, lone-pair electrons.[57] Therefore, the small fraction of unpaired electron spin density in the p_π-orbital is expected to have a minor influence on the value of the quadrupole coupling constant. Thus, the topa-semiquinone ^{14}N quadrupole coupling can be compared with quadrupole couplings of ^{14}N in crystallographically well-characterized diamagnetic molecules to infer the nuclear and electronic structure.

and the presence of a p_π-orbital that is indicated by the hyperfine tensor for the α-^{2}H interaction. The nitrogen atom therefore has an electron lone pair capable of hydrogen bond formation with an *in situ* proton donor. Indeed, hydrogen bonding by the nitrogen is indicated by the estimated nitrogen quadrupole coupling constant of 1.5 MHz in the topa-semiquinone in *Arthrobacter* methylamine oxidase[20] and the value of 1.5 ± 0.1 MHz estimated from the substrate ^{14}N ESEEM for bovine amine oxidase in ^1H_2O (K.W. and J.M. Unpublished). Values of the quadrupole coupling constant of <2.0 MHz are characteristic of trigonal nitrogen that is engaged in sharing of the lone-pair electrons (lone-pair orbital occupancies < 1.8).[32,58] Hydrogen bond formation is also consistent with the enhanced effective nuclear charge of the nitrogen atom suggested by the p_π-orbital contraction. To assist the assignment of features observed in the ENDOR spectra to an exchangeable proton that is hydrogen-bonded to the nitrogen (denoted N···H), the components of the dipolar tensor can be estimated by assuming that the hydrogen bond lies in the ring C–N–H plane and that $\rho_N = 0.24$ and $R_p = 0.68$ Å. A value for the N···H distance of $R = 1.5$ Å is obtained from the average from 22 organic crystals for hydrogen bonds to a nitrogen atom that is assumed to carry a formal positive charge.[59] The computed dipolar tensor is rhombic, with the following components: [–4.1, 6.3, –2.9] MHz. These values are in reasonable correspondence with the hyperfine couplings e–e′, f–f′, and g–g′ shown in Figure 7. The relatively weak intensities observed for these turning point features are consistent with the high anisotropy of the computed tensor. Therefore, we assign these hyperfine couplings to a proton that is involved in a hydrogen bond to the nitrogen atom, as shown in Tables 1 and 2.

The signs of the components are derived by considering the sign of A_{iso} to be negative, as for a covalently bonded proton.[45] Using this criterion, there is only one combination of signs of the principal values that approaches agreement with the computed dipolar tensor components. As shown in Table 2, the value of $A_{iso} = -0.4$ MHz suggests a small degree of covalent character in the N···H interaction.

C. Hydrogen Bond Interactions with the Oxygen Atoms. ^{1}H CW-ENDOR spectroscopy has previously shown that solvent protons that are hydrogen-bonded to semiquinone oxygen atoms in model systems are characterized by nearly pure dipolar hyperfine tensors.[24] Predominantly dipolar coupling has also been found for protons attached to protein residues that are hydrogen-bonded to the ubisemiquinone bound in redox catalytic protein sites,[55,60] as well as for enzyme catalytic tyrosine radicals.[61] The principal components of the dipolar hyperfine tensor are denoted $A_\perp$ and $A_\parallel$ and are equal to $-A_{dip}$ and $+2A_{dip}$, where A_{dip} is the dipolar coupling constant in the axially symmetric hyperfine field.[45] A pure dipolar coupling exhibits two pairs of turning point features in the ENDOR powder line shape when the spectrum is recorded in derivative mode. For $\nu < \nu_N$, a derivative-shaped feature with relatively strong intensity and a prominent positive excursion is expected at $\nu_N - A_\perp/2$, with a weaker, positive, peak-shaped feature at $\nu_N - A_\parallel/2$ ($=\nu_N - A_\perp$). For $\nu > \nu_N$, the form is maintained with the signs of the amplitude excursions reversed.

Two pairs of hyperfine couplings could be identified from those remaining after assignment of the N···H hydrogen bond tensor that conformed to the line shapes, relative intensities, and characteristic dipolar tensor proportions described above. These tensors are assigned to interactions with a proton hydrogen-bonded to each oxygen atom, denoted as O_A and O_B in Tables 1 and 2. These assignments are consistent with the conclusion that the oxygen atoms in the topa-semiquinone are deprotonated.

D. Absence of Intra-Cofactor Hydrogen Bond Interactions. The possibility exists for an intra-cofactor hydrogen bond between the trigonal nitrogen atom and an *ortho*-substituted oxygen atom.[52] A signature of intramolecular hydrogen bonding in radicals appears to be a substantial isotropic component to the hyperfine coupling of the hydrogen-bonded proton.[62] For example, in the 1,4,5,8-tetrahydroxynaphthalene cationic semiquinone, hyperfine coupling with two internally hydrogen bonded protons has $A_{iso} = |2.2|$ MHz with an unpaired spin density of ~0.1 on each oxygen atom.[62] Since the two weakest hyperfine interactions presented in Table 2 have negligible isotropic coupling, this suggests that there is no significant intra-cofactor hydrogen bonding in the topa-semiquinone. Hydrogen bonds to the topa-semiquinone are therefore supplied by protein heteroatoms or *in situ* water molecules.

Exchangeable Matrix Contributions. The sensitivity of the ^{1}H ENDOR matrix line to ^2H_2O exchange in enzyme-bound paramagnetic centers provides a qualitative assessment of the accessibility of the site to bulk, or high concentrations of localized, water.[23a] The line at the free ^{2}H nuclear frequency in ESEEM spectra has also been used to assess solvent accessibility.[63] The ^{1}H CW-ENDOR results obtained at 150-kHz FM show that there is a negligible (2%) difference in the maximum peak-to-trough derivative amplitude of the ^{1}H ENDOR signal after ^2H_2O exchange. Although the relative amplitude of the ^{2}H matrix line in the three-pulse ESEEM spectra is large, it is <5% as intense as the ^{2}H matrix line observed at comparable microwave frequency and τ values for model tyrosine radicals in aqueous glasses prepared by using ^2H_2O (K.W. and J. M. Unpublished). Thus, the unpaired spin density on the semiquinone is well-sequestered from the bulk aqueous solvent and high concentrations of local water. These findings are corroborated by the findings of Janes et al.,[6] which suggest that the active site is buried in the protein interior, as follows: (a) The visible absorption maximum for the protein-bound topa-quinone–phenylhydrazine adduct relative to model adducts prepared in solution exhibits bathochromic shifts of 10–16 nm, which are characteristic of a move from a polar, aqueous environment to the protein interior. (b) Incubation of the enzyme in the presence of the powerful denaturant, urea, at concentrations of 2 M was required to optimize the yield of peptide digestions of amine oxidase to release the pentapeptide fragment containing the phenylhydrazine-derivatized cofactor. The isolation of the cofactor from contact with the solvent suggests that a key role of the protein in promoting the efficiency of catalysis is to prevent uncontrolled access of solvent water molecules to labile Schiff-base and other catalytic intermediates.

Topa-semiquinone Structure and Implications for the Catalytic Mechanism. Figure 9 presents the structure of the topa-semiquinone in amine oxidase that is consistent with the results from the ^{2}H and ^{1}H ESEEM and CW-ENDOR spectroscopies. The rapid equilibrium formation of a significant concentration of the radical at room temperature[7,19] indicates that the oxidative phase of amine oxidation catalysis is optimized by direction through two reaction steps, involving single-electron transfers, that bracket a metastable intermediate, the topa-semiquinone. This two-barrier pathway follows a general pattern recognized in catalysis that avoids high activation barriers arising from concerted, large-amplitude motions of many atoms and uncom-

(57) (a) Townes, C. H.; Dailey, B. P. *J. Chem. Phys.* **1949**, *17*, 782–796. (b) Lucken, E. A. C. *Nuclear Quadrupole Coupling Constants*; Academic Press: London, 1969.

(58) (a) Hsieh, Y. N.; Rubenacker, G. V.; Cheng, C. P.; Brown, T. L. *J. Am. Chem. Soc.* **1977**, *99*, 1384–1389. (b) Ashby, C. I. H.; Cheng, C. P.; Brown, T. L. *J. Am. Chem. Soc.* **1978**, *100*, 6057–6063.

(59) Pimentel, G. C.; McClellan, A. L. *The Hydrogen Bond*; W. H. Freeman & Co.: San Francisco, CA, 1960.

(60) (a) Lubitz, W.; Abresch, E. C.; Debus, R. J.; Isaacson, R. A.; Okamura, M. Y.; Feher, G. *Biochim. Biophys. Acta* **1985**, *808*, 464–469. (b) Salerno, J. C.; Osgood, M.; Liu, Y.; Taylor, H.; Scholes, C. P. *Biochemistry* **1990**, *29*, 6987–6993.

(61) Babcock, G. T.; El-Deeb, M. K.; Sandusky, P. O.; Whittaker, M. M.; Whittaker, J. W. *J. Am. Chem. Soc.* **1992**, *114*, 3727–3734.

(62) Bolton, J. R.; Carrington, A.; Todd, P. F. *Mol. Phys.* **1963**, *6*, 169–177.

(63) (a) Mims, W. B.; Davis, J. L.; Peisach, J. *Biophys. J.* **1984**, *45*, 755–766. (b) Mims, W. B.; Davis, J. L.; Peisach, J. *J. Magn. Reson.* **1990**, *86*, 273–292.

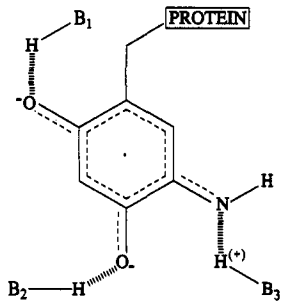

Figure 9. Structure of the topa-semiquinone intermediate in amine oxidase as revealed by ^2H and ^1H ESEEM and ^1H CW-ENDOR spectroscopies. The depicted positions of heteroatom ring substituents follow previous convention.[6,16] The positions of heteroatom ring substituents are at present unknown, but those shown here do not influence the conclusions drawn from the spectroscopic studies. Hatched lines represent hydrogen bond interactions. Dotted lines represent delocalized unpaired electron spin density. The formal charges on the *in situ* hydrogen bond donor groups, B_i, are not certain and are thus not explicitly included. As depicted, the charge on the radical is between −2 and −1, depending upon the degree of positive charge that arises from hydrogen bond formation with the nitrogen atom.

pensated charge density buildup along the reaction coordinate.[64] Our results illustrate aspects of this catalytic strategy at work at the molecular level.

The proton-transfer events that occur upon transformation of the aminohydroquinone into an iminoquinone species are associated with the first one-electron oxidation step.[65] This could lower contributions from the topa cofactor and its active-site region to the activation barrier for the second, dioxygen-requiring redox reaction. For example, *ab initio* computations show that proton-transfer barriers can approach 20 kcal/mol depending upon the heteroatom–heteroatom distance and relative orientation,[67] and barriers of this magnitude have been obtained for proton transfers in solution and in protease enzyme active sites by using semiempirical calculations.[68] If, as appears reasonable, the protons involved in hydrogen bonding to the topa-semiquinone are derived from those associated covalently with the heteroatoms in the aminohydroquinone,[65] then the protein-based hydrogen-bonding groups in the vicinity of the oxygen atoms and the nitrogen atom assist conversion of the aminohydroquinone to the semiquinone by relieving localized charge buildup in the radical. Participation of the protein protonatable groups in the transition state for aminohydroquinone to semiquinone transformation would be consistent with their function as base catalysts. The three hydrogen bonds that we have identified between the active site and the cofactor might also provide constraints for precise control of the *in situ* positioning of the cofactor. We speculate that interchange of hydrogen bond donor/acceptor roles for the cofactor heteroatoms, as suggested by comparison of the topa-semiquinone model in Figure 9 with the structures depicted for other reaction intermediates,[6,16] could provide a means to tailor the cofactor position at different stages in the catalytic cycle.

The most remarkable aspect of the topa-semiquinone structure is displayed in the region of the active carbon center, shown as position 5 in Figure 1. The conversion of a covalently attached amine nitrogen proton (in the aminohydroquinone) to a hydrogen-bonded proton (in the semiquinone) is unexpected. In contrast, deprotonation of the semiquinone oxygen atoms is not surprising because of the low pK_a values of 4–6 reported for semiquinones.[49] Therefore, deprotonation of the semiquinone nitrogen atom points to a specific influence of the protein on the reaction mechanism. The active-site group that accepts and, we assume, retains the proton in the N···H hydrogen bond appears to play an essential role in the oxidative reaction. If the rough proximity of the nitrogen atom and this protein protonatable group is maintained through the final oxidation step, we suggest that this group could also perform as an acid catalyst[69] in the water addition reaction following semiquinone oxidation that is required for elimination of the nitrogen atom. The presence of a single proton covalently bonded to the substrate nitrogen atom, the trigonal nitrogen geometry, and the p_π-orbital overlap in the C–N bond indicate a nuclear and electronic structure at the active center of the cofactor that resembles that of the iminoquinone intermediate. This partial development of an iminoquinone structure at the active center in the semiquinone state appears to eliminate key electronic and nuclear rearrangements associated with the semiquinone-to-iminoquinone transformation, thus facilitating forward progress of the reaction.

Acknowledgment. This work was supported by NIH Grants GM-37300 (G.T.B.), GM-45795 (J.M.), and GM-27659 (D.M.D.).

(64) (a) Sykes, P. *Guidebook to Mechanism in Organic Chemistry*, 5th ed.; Longman: London, 1981. (b) Fersht, A. R. *Enzyme Structure and Mechanism*; W. H. Freeman & Co.: New York, 1985.

(65) The protonation state of the oxygen atoms in the aminohydroquinone is uncertain. Recent mechanistic proposals from Klinman's group include an anionic aminohydroquinone species.[14] This is supported by comparison of the time-resolved UV/visible spectra of a product species observed in stopped-flow kinetic measurements[14] with the protonation-state-dependent UV absorption maxima of benzohydroquinone species *in vitro*.[66] Therefore, it appears that the oxygen atoms mediate a single-proton transfer associated with the first one-electron-oxidation step, although a double-proton transfer remains possible.

(66) (a) Weast, R. C. *CRC Handbook of Chemistry and Physics*, 58th ed.; CRC Press: Boca Raton, FL, 1978. (b) Morrison, L. E.; Schelhorn, J. E.; Cotton, T. M.; Bering, C. L.; Loach, P. A. In *Function of Quinones in Energy Conserving Systems*; Trumpower, B. L., Ed.; Academic Press: New York, 1982; pp 35–58.

(67) (a) Scheiner, S. *Acc. Chem. Res.* **1985**, *18*, 174–180. (b) Cybulski, S. M.; Scheiner, S. *J. Am. Chem. Soc.* **1989**, *111*, 23–31.

(68) (a) Warshel, A. *Biochemistry* **1981**, *21*, 3167–3177. (b) Warshel, A. *Proc. Natl. Acad. Sci.* **1984**, *81*, 444–448.

(69) Jencks, W. P. In *Progress in Physical Organic Chemistry 2*; Cohen, S. G., Streitweiser, A., Jr., Taft, R. W., Eds.; Interscience Publishers: New York, 1964; pp 63–128.